Modeling of hydrogen storage in hydride-forming materials: Statistical thermodynamics

A. Ledovskikh,[1] D. Danilov,[2] W. J. J. Rey,[2] and P. H. L. Notten[1,3,*]
[1]*Eindhoven University of Technology, Den Dolech 2, 5600 MB Eindhoven, The Netherlands*
[2]*Eurandom, Den Dolech 2, 5600 MB Eindhoven, The Netherlands*
[3]*Philips Research Laboratories, Prof. Holstlaan 4, 5656 AA Eindhoven, The Netherlands*
(Received 21 February 2005; revised manuscript received 29 June 2005; published 13 January 2006)

A new lattice gas model has been developed, describing the hydrogen storage in hydride-forming materials. This model is based on the mean-field theory and Bragg-Williams approximation. To describe first-order phase transitions and two-phase coexistence regions, a binary alloy approach has been adopted. A complete set of equations describing pressure-composition isotherms and equilibrium electrode potential curves of hydride forming materials in both solid-solution and two-phase coexistence regions has been set up. The proposed model defines both the equilibrium pressure and equilibrium potential as explicit functions of the normalized hydrogen concentration, using eight physically well-defined parameters. Gibbs free energies, entropies, and phase diagrams of both model ($LaNi_yCu_{1.0}$) and commercial, MischMetal-based, AB_5-type materials at different compositions and temperatures have been simulated. Good agreement between experimental and theoretical results for the pressure-composition isotherms obtained in the gas phase and the equilibrium potential curves measured in electrochemical environment has been found in all cases.

DOI: 10.1103/PhysRevB.73.014106 PACS number(s): 64.60.Cn, 05.50.+q, 81.30.−t, 82.47.Cb

I. INTRODUCTION

Hydride-forming (MH) compounds are successfully employed as electrode materials in high energy density, Nickel-MetalHydride (NiMH) batteries, nowadays widely applied in many portable electronics and hybrid electrical vehicles (HEV).[1–5] Recently, it has been emphasized that efficient hydrogen storage via the gas phase is also one of the key factors, enabling the future hydrogen economy, which will be based on the extensive use of hydrogen-driven fuel cells in a wide range of stationary and portable applications.[6]

The first step of hydrogen storage via the gas phase is dissociation of hydrogen molecules at the solid-gas interface. The as-produced adsorbed hydrogen atoms are subsequently transported toward interstitial sites inside the solid M, inducing the absorption process. Fortunately, these reaction steps were found to be reversible for many hydrogen storage materials and hydrogen can therefore also be desorbed.[5–8] The overall reaction can be represented by

$$\mathbf{M} + \frac{1}{2}\mathbf{H}_2 \leftrightarrow \mathbf{MH}. \tag{1}$$

Evidently, a chemical equilibrium exists between hydrogen stored in the solid and that present in the gas phase, which is generally characterized by pressure-composition isotherms.

A typical pressure-composition absorption isotherm and accompanying phase diagram are schematically shown in the curves in Figs. 1(a) and 1(b), respectively.[8–12] During hydrogen absorption at low concentrations, a solid solution is formed, which is generally denoted as the α phase. In this concentration region, the partial hydrogen pressure ($P^{eq}_{H_2}$) is clearly dependent on the amount of stored hydrogen. After the hydrogen concentration has reached a certain critical value (x_α), phase transition occurs and the α phase is continuously transformed into the β phase. The pressure dependence in this two-phase coexistence region is generally characterized by a (sloping) plateau.[8,13] Phase transition is completed at x_β, and a solid solution is subsequently formed only by the β phase. This typical three-step process will play an important role in the present paper.

Hydrogen storage can also be accomplished electrochemically in strong alkaline electrolyte,[4,5] according to

$$\mathrm{M} + \mathrm{H_2O} + e^- \leftrightarrow \mathrm{MH} + \mathrm{OH}^-. \tag{2}$$

The operation principle of NiMH batteries is based on the latter reversible electrochemical process, and hydrogen storage is induced by a current-driven charge-transfer reaction. During hydrogen absorption both the equilibrium electrode potential (E^{eq}_{MH}) and $P^{eq}_{H_2}$ are changing. Equation (3) describes the fundamental relationship between these two parameters[4,12]

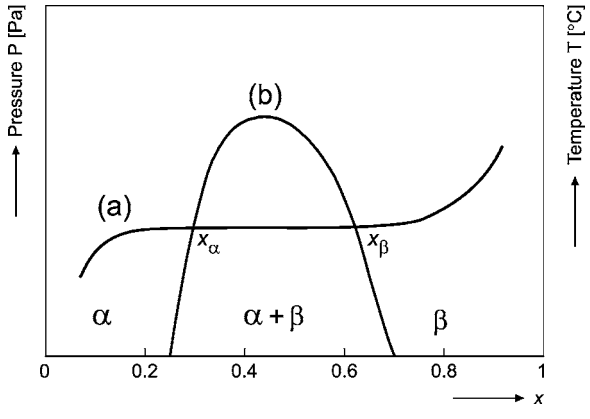

FIG. 1. General representation of a pressure-composition isotherm (a) and accompanying phase diagram (b) for a typical hydrogen storage material. The solid solutions for the α and β phases are indicated together with the temperature-dependent two-phase ($\alpha + \beta$) miscibility gap.

$$E_{\mathrm{MH}}^{eq} = -\frac{RT}{2F}\ln\frac{P_{\mathrm{H}_2}}{P_{\mathrm{ref}}}, \tag{3}$$

where the number of electrons involved in the charge-transfer process per hydrogen molecule (to be denoted as n_{H_2}) is equal to 2, F is the Faraday constant, E_{MH}^{eq} the equilibrium potential of the MH electrode, R the gas constant, T the temperature, P_{H_2} the equilibrium hydrogen pressure, and P_{ref} is the reference pressure of 1 bar $\cong 10^5$ Pa. Obviously, according to Eq. (3) the electrochemical equivalent of the gas-phase absorption isotherm resembles that shown in Fig. 1(a), as has been reported before.[4,5]

In line with the complex hydrogen absorption reaction sequence, the thermodynamics of the hydride-forming materials is also rather complex. Many attempts have been made to describe the absorption process and the resulting pressure-composition isotherms. The majority of the existing models employ methods of statistical mechanics, which allow obtaining macroscopic characteristics, such as Gibbs free energy and entropy, from a microscopic description of the system. Lacher[14] has proposed one of the early models. Unfortunately, this model produces nonphysical pressure-composition isotherms when fitted to the data with long sloping plateaus. Moreover, this model implies symmetry of the phase diagram.

An interesting approach has been proposed by Naito *et al.*[15] They also subjected a lattice gas model to statistical mechanics in order to describe pressure-composition isotherms with sloping plateaus. However, this model demonstrates a poor fit between the experimental and simulation results. The model of Lototsky *et al.*[16] is based on the work described by Lacher.[14] The authors took into account the asymmetry of the plateau region. Unfortunately, this model uses heuristic assumptions and parameters and has a high level of mathematical complexity. A simple absorption model has been proposed by McKinnon *et al.*[3,17] This model is also based on a lattice-gas, statistical mechanics approach. A Nernst-type equation for the equilibrium potential has been derived analytically, taking into account interaction energies between the absorbed hydrogen atoms.

In the present paper, a statistical lattice-gas model is proposed. This model is based on first principles of statistical mechanics and takes into account the hydrogen absorption and desorption in hydride-forming materials in both solid solution and two-phase coexistence regions. The simulated partial hydrogen pressure development and equilibrium electrode potential development are compared to experimental results.

II. MODEL

A. System definition

A well-known class of hydrogen storage alloys, nowadays exclusively applied in rechargeable NiMH batteries, is the so-called AB_5-type compounds. A schematic representation of the hexagonal unit cell of a nonstoichiometric representative of this class is shown in Fig. 2.[18–20] The crystallographic structure is composed of large A-type atoms (e.g., La) at the as-denoted 1*a* positions and smaller B-type atoms (e.g., Ni, Co) surrounding them in a well-defined way at the 3*g*, 2*c*, and 6l positions. Deviation from the stoichiometric composition was proven to take place by introducing dumbbell-pairs of B-type atoms at some A-type (2*e*) positions.[21,22]

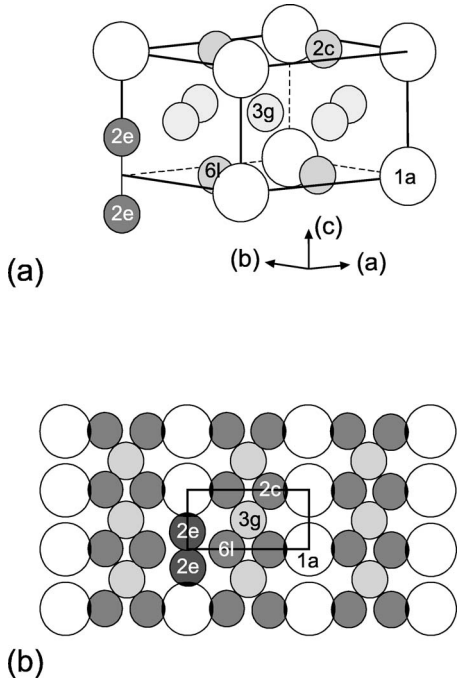

FIG. 2. Schematic representation of a nonstoichiometric AB_{5+x} unit cell (a) and corresponding cross-sectional view (b). The large and small atoms represent the A- and B-type atoms, respectively.[4]

Upon hydrogenation the hydrogen guest atoms will occupy certain well-defined interstitial sites in the open AB_5-host structure, which can be recognized in the crosssection of Fig. 2(b). It is assumed that a single guest atom can only occupy one host site and that each unit cell may have several host sites. Since the host material can be in more than one crystallographic state, different unit cells, each characterized by its own specific number of host sites, have to be considered.

It is well known that upon hydrogen absorption the volumetric crystal lattice expansion can be significant, generating a lot of mechanical stress in the solid. This is most pronounced in the two-phase coexistence region.[4,19] A schematic representation of this lattice expansion in the two-phase region is shown in Fig. 3. The volume expansion difference between the α and β phase can be quite substantial. Bulk materials often turn into powders due to these large mechanical stresses.[20] The two phases, which not necessarily need to have the same crystallographic structure, are separated by a small transition region. In the case of the present AB_5 materials, however, both phases have the same (hexagonal) crystal structure, although it should be noted that the dimensions of the unit cells are quite different.[4,19] Some hydrogen atoms are also schematically indicated in Fig. 3 (not drawn to scale). It is evident that the number of unit cells and hence the number of absorbed hydrogen atoms in these phases is strongly dependent on the overall hydrogen content.

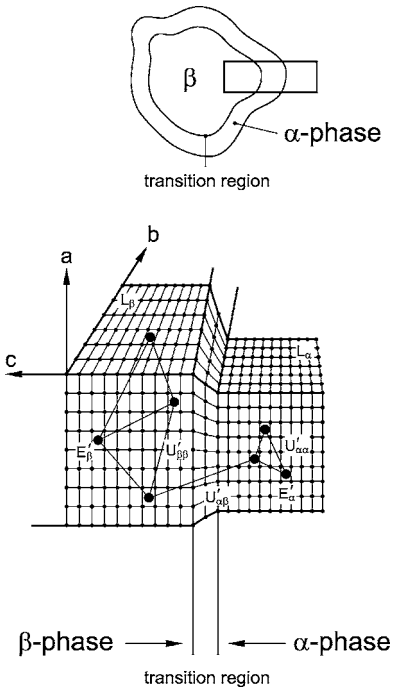

FIG. 3. Schematic representation of the lattice gas model in the two-phase ($\alpha+\beta$) coexistence region for a typical hydrogen storage material. The various host energies (L_i), hydrogen guest energies (E_i'), and interaction energies (U_{ij}') between hydrogen stored in the different phases (i,j) are indicated.

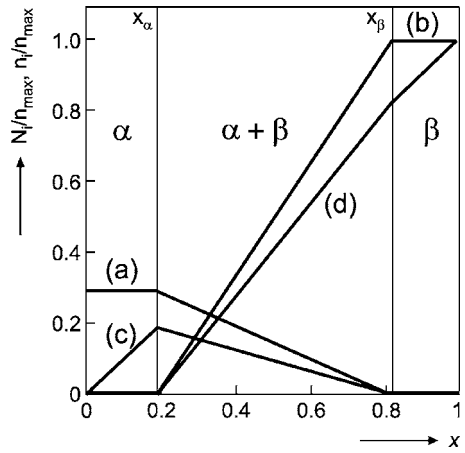

FIG. 4. Crystallographic implications of the hydride formation-decomposition mechanism for a material characterized by an α-to-β phase transition. The number of host sites [(a) and (b)] and the number of absorbed hydrogen atoms [(c) and (d)] in both the α [(a) and (c)] and β phase [(b) and (d)] are schematically represented by N_i and n_i, respectively, and are dependent on the hydrogenation-decomposition conditions and on the materials composition.

Consider a solid consisting of M unit cells, which can, upon hydrogen storage, be either in the $\alpha(M_\alpha)$ or the β state (M_β), leading to

$$M = M_\alpha + M_\beta. \tag{4}$$

When the crystallographic structure of both phases is assumed to be identical, which is the case for many AB_5-type hydride-forming compounds, M remains constant throughout the absorption-desorption process. The number of host sites per unit cell for the α and β phase are represented by d_α and d_β, respectively. For the β phase, this number is generally larger. The ratio, denoted by $d=d_\beta/d_\alpha$, is therefore larger or equal than 1. The total number of host sites in the solid (N) can then be obtained from

$$N = N_\alpha + N_\beta = d_\alpha M_\alpha + d_\beta M_\beta. \tag{5}$$

The amount of hydrogen guest atoms in the α and β phase is represented by n_α and n_β, respectively, where the total number of occupied hydrogen sites (n) is given by the summation of n_α and n_β. If the maximum number of host sites that can be occupied by hydrogen is defined by $n_{\max}$, the normalized number of absorbed hydrogen atoms (x) in the system can be represented by

$$x = \frac{n}{n_{\max}} = \frac{n_\alpha + n_\beta}{n_{\max}}. \tag{6}$$

The curves in Figs. 4(a) and 4(b) show the development of the normalized number of host sites ($N_i/n_{\max}$) as a function of the hydrogen content in the various phases (i) of the hydride-forming material. Obviously, both N_α [curve in Fig. 4(a)] and N_β [curve in Fig. 4(b)] remain constant in the solid-solution regions of the $\alpha(0 \leqslant x \leqslant x_\alpha)$ and β phase $(x_\beta \leqslant x \leqslant 1)$, respectively, whereas N_α decreases linearly and N_β increases linearly with increasing x in the two-phase region $(x_\alpha \leqslant x \leqslant x_\beta)$. The dependence of N_α and N_β on x in the three distinct hydrogen storage regions can therefore, in mathematical terms, be represented by

$$N_\alpha = \begin{cases} d_\alpha M & x < x_\alpha \\ d_\alpha M\left(\frac{x_\beta - x}{x_\beta - x_\alpha}\right), & \text{if } x_\alpha \leqslant x \leqslant x_\beta \\ 0 & x > x_\beta \end{cases}, \tag{7}$$

$$N_\beta = \begin{cases} 0 & x < x_\alpha \\ d_\beta M\left(\frac{x - x_\alpha}{x_\beta - x_\alpha}\right), & \text{if } x_\alpha \leqslant x \leqslant x_\beta \\ d_\beta M & x > x_\beta \end{cases}.$$

The development of the normalized number of absorbed guest hydrogen atoms ($n_i/n_{\max}$) is also shown in Fig. 4. It is clear that during the initial stages of the absorption process the hydrogen atoms start to fill the available α-host sites only [curve in Fig. 4(c)]. The maximum level is reached at x_α. Not necessarily all available host sites in the α phase have to be filled up before phase transition is induced, as the example of Fig. 4 indicates. Subsequently, n_α starts to decrease linearly in the two-phase coexistence region to become zero at x_β. Simultaneously, n_β increases linearly [curve in Fig. 4(d)]. Finally, at x_β, there are no α sites available anymore and phase transition is completed. All available host sites are assumed fully occupied by hydrogen atoms in the present example, i.e., $n_\beta = N_\beta = n_{\max}$ at $x=1$. Evidently, $n(=n_\alpha+n_\beta)$increases linearly with x over the entire concentration range from 0 up to 1. Therefore, the following expres-

sions for n_α and n_β are considered in the three distinct hydrogen storage regions

$$n_\alpha = \begin{cases} xn_{\max} & x < x_a \\ x_\alpha n_{\max}\left(\dfrac{x_\beta - x}{x_\beta - x_\alpha}\right), & \text{if } x_\alpha \leqslant x \leqslant x_\beta \\ 0 & x > x_\beta \end{cases},$$

$$n_\beta = \begin{cases} 0 & x < x_\alpha \\ x_\beta n_{\max}\left(\dfrac{x - x_\alpha}{x_\beta - x_\alpha}\right), & \text{if } x_\alpha \leqslant x \leqslant x_\beta \\ xn_{\max} & x > x_\beta \end{cases}. \quad (8)$$

B. Energy description

The Gibbs free energy (G) of the present hydrogen storage system can, in general terms, be represented by[23]

$$G = H - TS = U + PV - TS, \quad (9)$$

where H is the enthalpy, S the entropy, U the energy of the hydrogen storage system, and P is the pressure. The relationship between the Gibbs free energy and the partial hydrogen pressure can be represented by[4,12]

$$\Delta G_{\mathrm{MH}} = \frac{kT}{2}\ln\frac{P_{\mathrm{H_2}}}{P_{\mathrm{ref}}} \quad (10)$$

where k is the Boltzmann constant ($k = 1.38 \times 10^{-23}$ J/K $\equiv 8.62 \times 10^{-5}$ eV/K). As the change in Gibbs free energy (ΔG_{MH}) is expressed per absorbed hydrogen atom, $n_{\mathrm{H_2}} = 2$ is included in Eq. (10). The relationship between the Gibbs free energy of the electrochemical reaction and E^{eq}_{MH} is given by[3,4,12]

$$\Delta G_{\mathrm{MH}} = -eE^{eq}_{\mathrm{MH}}. \quad (11)$$

in which e is the electronic charge and, in accordance with Eq. (2), the number of electrons involved in the charge transfer process per one hydrogen atom (n_H) is taken as 1. Taking into account the Avogadro number (N_A) and that $eN_A = F$ and $kN_A = R$, indeed shows the validity of the relationship between E^{eq}_{MH} and P_{H_2} [Eq. (3)].

Evidently, the Gibbs free energy of the entire system in Eq. (9) changes when the number of absorbed hydrogen atoms n changes. As G depends on n via $x = n/n_{\max}$, G can be considered a function of x. By definition, ΔG [Eqs. (10) and (11)] is an increment of the Gibbs free energy of the system when the number of intercalated hydrogen atoms n is increased by 1. Assuming differentiability of G, we may write[24]

$$\Delta G = G(x + \Delta x) - G(x) = \frac{\partial G}{\partial x}\Delta x + r_x(\Delta x) = \frac{\partial G}{\partial x}\frac{1}{n_{\max}} + r_x(\Delta x), \quad (12)$$

where $\Delta x = 1/n_{\max}$ and $r_x(\Delta x)$ is the residual term of order smaller than Δx. As $n_{\max}$ is usually very large for practical systems, Δx is very small. Consequently, the residual term $r_x(\Delta x)$ can be neglected, leading to $\Delta G = (\partial G/\partial x)/n_{\max}$. Taking Eq. (9) into account, we obtain

$$\Delta G = \left(\frac{\partial U}{\partial x} + V\frac{\partial P}{\partial x} + P\frac{\partial V}{\partial x} - S\frac{\partial T}{\partial x} - T\frac{\partial S}{\partial x}\right)\frac{1}{n_{\max}}. \quad (13)$$

In order to reduce the complexity of the present derivation, it is assumed that volume, temperature, and pressure changes do not have a significant impact on the total energy of the system and are considered to remain constant. Equation (13) then simplifies to a more convenient form

$$\Delta G = \left(\frac{\partial U}{\partial x} - T\frac{\partial S}{\partial x}\right)\frac{1}{n_{\max}}. \quad (14)$$

To describe the energy of the present hydrogen absorption system, a few aspects must be taken into account. First, the energy of the various host crystal lattices has to be considered. The contribution of each unit cell to the total energy is denoted as L_α and L_β for the α and β phase, respectively.[25,26] Second, the so-called Bragg-Williams approximation has been adopted, implying that the absorbed hydrogen atoms are randomly distributed in the hydride-forming material.[27] This is schematically depicted in Fig. 3. In the case of two-phase coexistence, two energetically different types of host sites coexist in the system and a binary alloy approach must be adopted. E'_α and E'_β represent the energy of absorbed hydrogen in both phases. It is, furthermore, assumed that an absorbed hydrogen atom at a particular site can interact with a hydrogen atom at any other site,[2,3] with specific interaction energy (U'_{ii}). According to the mean-field approximation,[27] the interaction energy between the occupied sites does not depend on their distance. $U'_{\alpha\alpha}$ and $U'_{\beta\beta}$ are the interaction energies between two absorbed atoms in the α and β phase, respectively, and $U'_{\alpha\beta}$ represents the interaction energy between two absorbed hydrogen atoms in different phases.[27] The various interaction energies between absorbed hydrogen atoms are also schematically indicated in Fig. 3. These considerations lead to the following Hamiltonian (U) for the entire hydrogen storage system

$$U = L_\alpha M_\alpha + L_\beta M_\beta + E'_\alpha n_\alpha + E'_\beta n_\beta + \frac{U'_{\alpha\alpha}}{2n_{\max}}n_\alpha^2 + \frac{U'_{\beta\beta}}{2n_{\max}}n_\beta^2 + \frac{U'_{\alpha\beta}}{2n_{\max}}n_\alpha n_\beta. \quad (15)$$

Taking into account the definition of M_α and M_β in Eqs. (4) and (5), the first two terms in Eq. (15) can be rewritten as

$$L_\alpha M_\alpha + L_\beta M_\beta = L_\alpha M + (L_\beta - L_\alpha)M_\beta = L_\alpha M + \frac{(L_\beta - L_\alpha)N_\beta}{d_\beta}. \quad (16)$$

From a mathematical point of view, it is convenient to write the Gibbs free energy and its contributions in terms of $x(=n/n_{\max})$. Substituting N_β, according to Eq. (7), and replacing n_α and n_β for x by means of Eq. (8), the following relationships are obtained for the three considered crystallographic regions

$$U = n_{\max}\begin{cases} \frac{L_\alpha M}{n_{\max}} + E'_\alpha x + \frac{U'_{\alpha\alpha}}{2}x^2 & x < x_\alpha \\ \frac{L_\alpha}{d_\beta} + \frac{(L_\beta - L_\alpha)}{d_\beta}\left(\frac{x-x_\alpha}{x_\beta - x_\alpha}\right) + E'_\alpha x_\alpha\left(\frac{x_\beta - x}{x_\beta - x_\alpha}\right) + E'_\beta x_\beta\left(\frac{x-x_\alpha}{x_\beta - x_\alpha}\right) + \frac{U'_{\alpha\alpha}x_\alpha^2}{2}\left(\frac{x_\beta - x}{x_\beta - x_\alpha}\right)^2 + \frac{U'_{\beta\beta}x_\beta^2}{2}\left(\frac{x-x_\alpha}{x_\beta - x_\alpha}\right)^2 + \frac{U'_{\alpha\beta}x_\alpha x_\beta}{2}\left(\frac{x-x_\alpha}{x_\beta - x_\alpha}\right)\left(\frac{x_\beta - x}{x_\beta - x_\alpha}\right) & x_\alpha \leqslant x \leqslant x_\beta \\ \frac{L_\beta M}{n_{\max}} + E'_\beta x + \frac{U'_{\beta\beta}}{2}x^2 & x > x_\beta \end{cases} \tag{17}$$

Differentiating Eq. (17) with respect to x ultimately leads to

$$\frac{\partial U}{\partial x} = e n_{\max}\begin{cases} E_\alpha + U_{\alpha\alpha}x & x < x_\alpha \\ \left(E_\beta x_\beta - E_\alpha x_\alpha - U_{\alpha\alpha}x_\alpha^2\frac{x_\beta - x}{x_\beta - x_\alpha} + U_{\beta\beta}x_\beta^2\frac{x-x_\alpha}{x_\beta - x_\alpha} + \frac{U_{\alpha\beta}}{2}\frac{x_\alpha x_\beta}{x_\beta - x_\alpha}[(x_\beta - x) - (x - x_\alpha)] + L\right)/(x_\beta - x_\alpha) & x_\alpha \leqslant x \leqslant x_\beta \\ E_\beta + U_{\beta\beta}x & x > x_\beta \end{cases} \tag{18}$$

in which the primed constants are redefined as

$$E_\alpha = \frac{E'_\alpha}{e}, \quad E_\beta = \frac{E'_\beta}{e}, \quad U_{\alpha\alpha} = \frac{U'_{\alpha\alpha}}{e}, \quad U_{\beta\beta} = \frac{U'_{\beta\beta}}{e}, \quad U_{\alpha\beta} = \frac{U'_{\alpha\beta}}{e}$$

and L is replaced by

$$L = \frac{L_\beta - L_\alpha}{e d_\beta}. \tag{19}$$

The transitions from the primed symbols (E'_i, U'_i) to the unprimed symbols (E_i, U_i) imply dimensional transformation from joules to electronvolts.

To calculate the entropy contributions, the Boltzmann equation was adopted[2,3]

$$S_i = k \ln W_i \tag{20}$$

where the thermodynamic integral (W_i) is given by

$$W_i = \frac{N_i!}{n_i!\,(N_i - n_i)!}. \tag{21}$$

N_i and n_i again refer to the number of host and guest sites, respectively, in phase (i). The total entropy of the system S is the sum of entropies of both phases $S = S_\alpha + S_\beta$. Using the Stirling approximation,

$$\ln N_i! \approx N_i \ln N_i - N_i \text{ and } \ln n_i! \approx n_i \ln n_i - n_i \tag{22}$$

the approximate expansion of the logarithmic form of the thermodynamic integral can be written as

$$\begin{aligned} \ln W_i &\approx N_i \ln N_i - N_i - n_i \ln n_i + n_i \\ &\quad - (N_i - n_i)\ln(N_i - n_i) + N_i - n_i \\ &= N_i \ln N_i - n_i \ln n_i - (N_i - n_i)\ln(N_i - n_i) \\ &= -N_i\left[\frac{n_i}{N_i}\ln\frac{n_i}{N_i} + \left(1 - \frac{n_i}{N_i}\right)\ln\left(1 - \frac{n_i}{N_i}\right)\right] \end{aligned} \tag{23}$$

and a general expression for S_i is obtained for the entropy of each phase, according to

$$S_i \approx -kN_i\left[\frac{n_i}{N_i}\ln\frac{n_i}{N_i} + \left(1 - \frac{n_i}{N_i}\right)\ln\left(1 - \frac{n_i}{N_i}\right)\right]. \tag{24}$$

Replacing both n_i and N_i in Eq. (24) by means of Eqs. (7) and (8) and using the fact that $n_{\max}/(d_\alpha M) = d$ and $n_{\max}/(d_\beta M) = 1$, the following expression for the total entropy is obtained in the three considered solid-state regions:

$$S = -kn_{\max}\begin{cases} \dfrac{xd\ln(xd) + (1 - xd)\ln(1 - xd)}{d} & x < x_\alpha \\ \dfrac{S^0_\alpha}{d}\left(\dfrac{x_\beta - x}{x_\beta - x_\alpha}\right) + S^0_\beta\left(\dfrac{x - x_\alpha}{x_\beta - x_\alpha}\right) & \text{if } x_\alpha \leqslant x \leqslant x_\beta \\ x\ln x + (1 - x)\ln(1 - x) & x > x_\beta \end{cases}, \tag{25}$$

in which

$$S_\alpha^0 = x_\alpha d \ln(x_\alpha d) + (1 - x_\alpha d)\ln(1 - x_\alpha d) \tag{26}$$

$$S_\beta^0 = x_\beta \ln x_\beta + (1 - x_\beta)\ln(1 - x_\beta).$$

Differentiating Eq. (25) with respect to x and, in accordance with Eq. (14), multiplying with $-T$ leads to

$$-T\frac{\partial S}{\partial x} = -kTn_{\max}\begin{cases} \ln\left(\dfrac{1-xd}{xd}\right) & x < x_\alpha \\ \left(\dfrac{S_\alpha^0}{d} - S_\beta^0\right)/(x_\beta - x_\alpha), & \text{if } x_\alpha \leqslant x \leqslant x_\beta \\ \ln\left(\dfrac{1-x}{x}\right) & x > x_\beta \end{cases} \tag{27}$$

The summation of Eqs. (18) and (27) ultimately leads to the general expression for ΔG_{MH} expressed in electronvolts per atom H in the three considered crystallographic regions

$$\Delta G_{\mathrm{MH}} = \begin{cases} e(E_\alpha + U_{\alpha\alpha}x) - kT\ln\left(\frac{1-xd}{xd}\right) \\ \frac{e}{x_\beta - x_\alpha}\left\{-E_\alpha x_\alpha - U_{\alpha\alpha}x_\alpha^2\left(\frac{x_\beta - x}{x_\beta - x_\alpha}\right) + E_\beta x_\beta + U_{\beta\beta}x_\beta^2\left(\frac{x - x_\alpha}{x_\beta - x_\alpha}\right) + \frac{U_{\alpha\beta}}{2}\left(\frac{x_\alpha x_\beta}{x_\beta - x_\alpha}\right)[(x_\beta - x) - (x - x_\alpha)] + L\right\} - \frac{kT}{(x_\beta - x_\alpha)}\left(\frac{S_\alpha^0}{d} - S_\beta^0\right) \\ e(E_\beta + U_{\beta\beta}x) - kT\ln\left(\frac{1-x}{x}\right) \end{cases} \tag{28}$$

Finally, considering Eq. (10) a set of expressions is obtained, describing pressure-composition isotherms

$$P_{\mathrm{H}_2} = P_{\mathrm{ref}}\exp\begin{cases} \frac{2e(E_\alpha + U_{\alpha\alpha}x)}{kT} - 2\ln\left(\frac{1-xd}{xd}\right) \\ \frac{\frac{2e}{kT}\left\{-E_\alpha x_\alpha - U_{\alpha\alpha}x_\alpha^2\left(\frac{x_\beta - x}{x_\beta - x_\alpha}\right) + E_\beta x_\beta + U_{\beta\beta}x_\beta^2\left(\frac{x - x_\alpha}{x_\beta - x_\alpha}\right) + \frac{U_{\alpha\beta}x_\alpha x_\beta}{2}\left(\frac{(x_\beta - x) - (x - x_\alpha)}{(x_\beta - x_\alpha)}\right) + L\right\} - 2\left(\frac{S_\alpha^0}{d} - S_\beta^0\right)}{(x_\beta - x_\alpha)} \\ \frac{2e(E_\beta + U_{\beta\beta}x)}{kT} - 2\ln\left(\frac{1-x}{x}\right) \end{cases} \tag{29}$$

Similarly, considering Eq. (11), the dependence of the electrode equilibrium potential on the hydrogen content is

$$E_{\mathrm{MH}}^{eq} = \begin{cases} \frac{kT}{e}\ln\left(\frac{1-xd}{xd}\right) - (E_\alpha + U_{\alpha\alpha}x) \\ \frac{\frac{kT}{e}\left(\frac{S_\alpha^0}{d} - S_\beta^0\right) - \left\{-E_\alpha x_\alpha - U_{\alpha\alpha}x_\alpha^2\left(\frac{x_\beta - x}{x_\beta - x_\alpha}\right) + E_\beta x_\beta + U_{\beta\beta}x_\beta^2\left(\frac{x - x_\alpha}{x_\beta - x_\alpha}\right) + \frac{U_{\alpha\beta}x_\alpha x_\beta}{2}\left[\left(\frac{x_\beta - x}{x_\beta - x_\alpha}\right) - \left(\frac{x - x_\alpha}{x_\beta - x_\alpha}\right)\right] + L\right\}}{(x_\beta - x_\alpha)} \\ \frac{kT}{e}\ln\left(\frac{1-x}{x}\right) - (E_\beta + U_{\beta\beta}x) \end{cases} \tag{30}$$

or in electrochemical terms, when $eN_A = F$ and $kN_A = R$ is taken into account

$$E_{\mathrm{MH}}^{eq} = \begin{cases} \frac{RT}{F}\ln\left(\frac{1-xd}{xd}\right) - (E_\alpha + U_{\alpha\alpha}x) \\ \frac{\frac{RT}{F}\left(\frac{S_\alpha^0}{d} - S_\beta^0\right) - \left\{-E_\alpha x_\alpha - U_{\alpha\alpha}x_\alpha^2\left(\frac{x_\beta - x}{x_\beta - x_\alpha}\right) + E_\beta x_\beta + U_{\beta\beta}x_\beta^2\left(\frac{x - x_\alpha}{x_\beta - x_\alpha}\right) + \frac{U_{\alpha\beta}x_\alpha x_\beta}{2}\left[\left(\frac{x_\beta - x}{x_\beta - x_\alpha}\right) - \left(\frac{x - x_\alpha}{x_\beta - x_\alpha}\right)\right] + L\right\}}{(x_\beta - x_\alpha)} \\ \frac{RT}{F}\ln\left(\frac{1-x}{x}\right) - (E_\beta + U_{\beta\beta}x) \end{cases} \tag{31}$$

According to the derivations, the resulting equilibrium potential is nonlinear in the solid-solution regions but linear during phase transition.[12,28,29] Both Eqs. (29) and (30) are, in principle, discontinuous at the phase transition points x_α and x_β. From common physical sense it is, however, obvious that the experimentally observed isotherms must be continuous. As only a limited number of data points are usually available from the experiments (see, e.g., Fig. 5) this does unfortunately not allow to estimate the various parameters with sufficient precision such that the simulated curve does not reveal any visible "kinks." In order to obtain a physically relevant subset of parameters, yielding continuous dependencies in Eqs. (29) and (30), some restrictions are imposed to the constants to preserve the continuity of $P_{H_2}(x)$ at x_α and x_β, namely,

$$\lim_{x\uparrow x_\alpha} P_{H_2}(x) = \lim_{x\downarrow x_\alpha} P_{H_2}(x) \quad \text{and} \quad \lim_{x\uparrow x_\beta} P_{H_2}(x) = \lim_{x\downarrow x_\beta} P_{H_2}(x). \tag{32}$$

Calculating the limits in Eq. (32) leads to the following two continuity equations

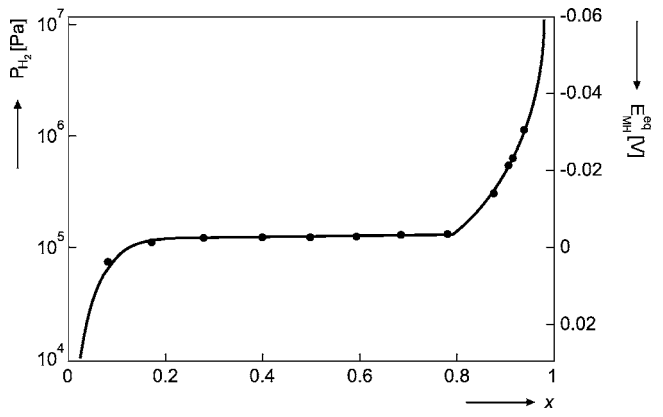

FIG. 5. Measured (symbols) and calculated (line) pressure-composition isotherm for $LaNi_{4.0}Cu_{1.0}$. The measurements have been performed via the gas phase 20 °C.[4,19]

$$D_\alpha - E_\alpha - U_{\alpha\alpha}x_\alpha = \frac{D_{\alpha\beta}}{x_\beta - x_\alpha} - \frac{1}{x_\beta - x_\alpha}\left(E_\beta x_\beta - E_\alpha x_\alpha - U_{\alpha\alpha}x_\alpha^2 + \frac{U_{\alpha\beta}}{2}x_\alpha x_\beta + L\right),$$

$$D_\beta - E_\beta - U_{\beta\beta}x_\beta = \frac{D_{\alpha\beta}}{x_\beta - x_\alpha} - \frac{1}{x_\beta - x_\alpha}\left(E_\beta x_\beta - E_\alpha x_\alpha + U_{\beta\beta}x_\beta^2 - \frac{U_{\alpha\beta}}{2}x_\alpha x_\beta + L\right), \quad (33)$$

where

$$D_\alpha = \frac{kT}{e}\ln\left(\frac{1 - x_\alpha d}{x_\alpha d}\right), \quad D_\beta = \frac{kT}{e}\ln\left(\frac{1 - x_\beta}{x_\beta}\right),$$

$$D_{\alpha\beta} = \frac{kT}{e}\left(\frac{S_\alpha^0}{d} - S_\beta^0\right).$$

Solving Eq. (33) with respect to L and $U_{\alpha\beta}$ results in

$$L = D_{\alpha\beta} - E_\beta x_\beta + E_\alpha x_\alpha + \frac{U_{\alpha\alpha}x_\alpha^2 - U_{\beta\beta}x_\beta^2}{2} - \{D_\alpha + D_\beta - (E_\alpha + E_\beta) - (U_{\alpha\alpha}x_\alpha + U_{\beta\beta}x_\beta)\}\frac{(x_\beta - x_\alpha)}{2}, \quad (34)$$

$$U_{\alpha\beta} = \frac{U_\alpha x_\alpha^2 + U_{\beta\beta}x_\beta^2}{x_\alpha x_\beta} - \frac{D_\alpha - D_\beta - E_\alpha + E_\beta - U_{\alpha\alpha}x_\alpha + U_{\beta\beta}x_\beta}{x_\alpha x_\beta}(x_\beta - x_\alpha).$$

Equations (29)–(31) together with the restrictions of Eq. (34) form the final result. It should be emphasized that the continuity conditions are necessary to preserve the continuity of both P_{H_2} [Eq. (29)] and $E_{MH}^{eq}(x)$ [Eqs. (30) and (31)], while the Gibbs free energy of the system is always continuous, independent of the conditions given by Eq. (33).

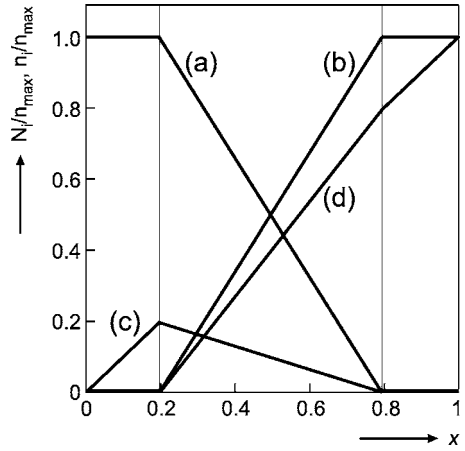

FIG. 6. Simulated development of the number of host sites (N_i) [(a) and (b)] and hydrogen guest sites (n_i) [(c) and (d)] during hydrogen absorption in $LaNi_{4.0}Cu_{1.0}$ at 20 °C (see corresponding isotherm of Fig. 5). Note that in this specific case the crystallographic structure of both phases are identical and that $d_\alpha = d_\beta = 1$.

III. RESULTS AND DISCUSSION

The presented lattice-gas model has been tested, using the experimental data reported for various AB_5-type hydrogen storage materials. These materials have been thoroughly characterized with respect to their physical and electrochemical performance. The isotherms for both model-type materials and commercial, MischMetal-based, hydride-forming materials have been simulated as a function of composition and temperature, respectively. Since all considered materials have the same, hexagonal, crystallographic structure for both the α and β phase it is evident that the number of host sites per unit cell remains constant, i.e., parameter d is considered unity in the present simulations.

It is well known that nonstoichiometric hydride-forming materials are stable with respect to electrochemical hydrogen storage.[18,19] The crystallographic structure of these materials has been illustrated in Fig. 2. These stable compounds are more attractive than conventional AB_5 alloys as they exclude expensive Co. In addition, these materials have a rather simple composition and can therefore be considered as model systems for which the phase transitions can be well controlled by the stoichiometric composition.

Figure 5 shows the agreement between the experimentally measured (symbols) and simulated (line) pressure-composition isotherm (left-hand axis) and the corresponding equilibrium potential curve (right-hand axis) for the stoichiometric $LaNi_{4.0}Cu_{1.0}$. In this specific stoichiometric case no dumbbell pairs have been introduced in the host crystal lattice (see Fig. 2). The experimental absorption isotherms have been measured with a conventional "Sieverts-type" apparatus by expanding a known amount of gas or vacuum into an *in situ* x-ray diffraction (XRD) cell and allowing the system to come to equilibrium after each pressure change.[19] The potential has been expressed with respect to the hydrogen reference electrode, i.e., 0 V corresponds to a partial hydrogen pressure of 1 bar ($\approx 10^5$ Pa). The *in situ* XRD measurements allowed obtaining crystallographic information of the

TABLE I. Simulation results for stoichiometric and non-stoichiometric, hydride-forming model materials

Composition	Experimental		Simulation							
	x_α	x_β	x_α	x_β	E_α (eV)	E_β (eV)	$U_{\alpha\alpha}$ (eV)	$U_{\beta\beta}$ (eV)	$U_{\alpha\beta}$ (eV)	L (eV)
$LaNi_{4.0}Cu_{1.0}$	0.11	0.76	0.196	0.794	0.069	0.011	−0.158	−0.053	−0.257	0.020
$LaNi_{4.2}Cu_{1.0}$	0.19	0.67	0.231	0.711	0.070	0.017	−0.139	−0.042	−0.181	0.017
$LaNi_{4.4}Cu_{1.0}$	0.33	0.41	0.276	0.448	0.072	0.056	−0.122	−0.080	−0.206	0.003
$LaNi_{5.0}Cu_{1.0}$	0.36	0.36	0.346	0.346	0.046	0.069	−0.026	−0.092		−0.003

system as a function of the hydrogen content. The solid line represents the simulation according to Eq. (29). The numerical values of the parameters x_α, x_β, E_α, E_β, $U_{\alpha\alpha}$, $U_{\beta\beta}$, and $U_{\alpha\beta}$ were obtained by nonlinear least-squares method and are listed in Table I. As Fig. 5 reveals, the lattice-gas model describes the isotherm quite well for the stoichiometric $LaNi_{4.0}Cu_{1.0}$ material. Three regions can be clearly distinguished: a Nernst-type solid-solution region at low hydrogen concentration ($x<0.196$), a long, almost flat, two-phase coexistence plateau region ($0.196\leqslant x\leqslant 0.794$), and a Nernst-type solid-solution region at high hydrogen concentration ($x>0.794$).

The presented lattice-gas model can now provide much more detailed information about the structure of the hydride-forming material and the phase-transition process. Curves in Fig. 6(a) and 6(b), for example, illustrates the changes in the normalized number of available host sites and absorbed hydrogen atoms in the various crystallographic regions of $LaNi_{4.0}Cu_{1.0}$. As expected, the number of α host sites remains constant in the α solid solution ($x<0.196$) and decreases linearly to zero in the two-phase region [$0.196\leqslant x\leqslant 0.794$ in the curve Fig. 6(a)]. In the β solid-solution region, on the other hand, the number of α host sites is zero [curve in Fig. 6(b)]. The number of β host sites ($N_\beta/n_{\max}$) behaves exactly in the opposite way as the α sites because $N_\alpha+N_\beta=N=n_{\max}$. Similarly, the number of absorbed hydrogen atoms increases linearly in the α region, decreases linearly to zero in the two-phase region ($0.196\leqslant x\leqslant 0.794$) and remains zero in the β solid-solution region [curve in Fig. 6(c)]. Contrary, $n_\beta/n_{\max}$ is zero in the α solid-solution region, to increase linearly but with different slopes in the two-phase and β solid-solution regions [curve in Fig. 6(d)]. Again, this behavior is expected since $n_\alpha+n_\beta=n=xn_{\max}$.

Figure 7 shows the contribution of the energy U [curve in Fig. 7(a)] and the entropy $-TS$ [curve in Fig. 6(b)] to the total Gibbs free energy [curve in Fig. 6(c)], see also Eq. (9). Since L_α enters into the total Gibbs free energy as a constant additive term [see Eq. (17)], it has been assumed to be zero for simplicity. The contributions of both terms are of opposite signs and are approximately equal in magnitude. As expected, these contributions are continuous but not smooth and "kinks" are clearly visible at the phase transition points. It is interesting to see, how the energy contributions from Fig. 7 affect the corresponding voltage contributions, shown in Fig. 8. Evidently, the kinks of the energy terms now correspond to the jumps in the "differentiated" voltage curves [see Eqs. (30) and (31)]. The continuous behavior in the Gibbs free energy (Fig. 7) and the discontinuous behavior in the differentiated curve (e.g., Fig. 8) are in line with the definition of first-order phase-transitions. However, these jumps at the phase transition points are of equal magnitude and the equilibrium voltage is therefore continuous. The various curves of Fig. 8 show that the singularities of the equilibrium potential near $x=0$ and $x=1$ are clearly caused by the entropy related, Nernstian, terms. It is more complex to draw conclusions from the voltage contributions in the plateau region (Fig. 8), but a more detailed inspection of Fig. 7 reveals that the upward slope of the Gibbs free energy is mainly caused by an increase of the energy [curve in Fig.

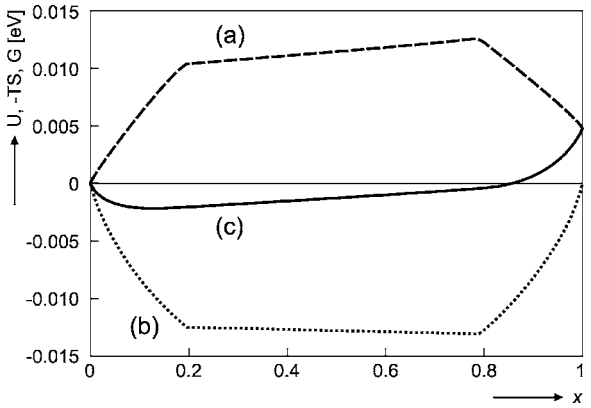

FIG. 7. Calculated energy (a) and entropy (b) contribution to the total Gibbs free energy (c) upon hydrogenation of the $LaNi_{4.0}Cu_{1.0}$ system (see corresponding isotherm of Fig. 5).

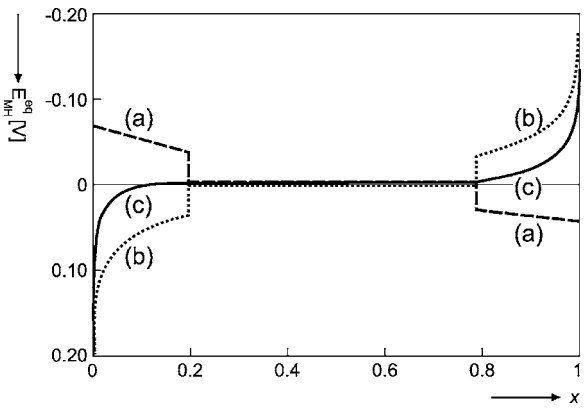

FIG. 8. Calculated energy (a) and entropy (b) contribution to the total equilibrium voltage (c) upon hydrogenation of the $LaNi_{4.0}Cu_{1.0}$ system (see corresponding isotherm of Fig. 5).

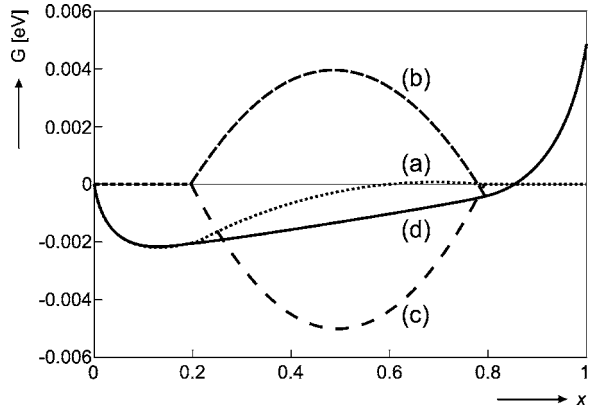

FIG. 9. Calculated contributions of the α-phase (a), β-phase (b), and interphase interaction (c) energy to the total change of the Gibbs free energy (d) along the pressure-composition isotherm of the $LaNi_{4.0}Cu_{1.0}$(see corresponding isotherm of Fig. 5). In the α solid-solution region only (a) contribution is nonzero and equal to $E_\alpha x + U_{\alpha\alpha}x^2/2 + RT[dx\ln(dx) + (1-dx)\ln(1-dx)]/(Fd)$. In the β solid-solution region only (b) contribution is nonzero and equal to $E_\beta x + U_{\beta\beta}x^2/2 + RT[x\ln(x) + (1-x)\ln(1-x)]/F + L$. In the two-phase region the contributions are determined as

$$(a)\quad E_\alpha x_\alpha[(x_\beta - x)/(x_\beta - x_\alpha)] + U_{\alpha\alpha}x_\alpha^2/2[(x_\beta - x)/(x_\beta - x_\alpha)]^2 + RTS_\alpha^0[(x_\beta - x)/(x_\beta - x_\alpha)]/(Fd),$$

$$(b)\quad E_\beta x_\beta[(x - x_\alpha)/(x_\beta - x_\alpha)] + U_{\beta\beta}x_\beta^2/2[(x - x_\alpha)/(x_\beta - x_\alpha)]^2 + RTS_\beta^0[(x - x_\alpha)/(x_\beta - x_\alpha)]/F + L[(x - x_\alpha)/(x_\beta - x_\alpha)],$$

and

$$(c)\quad U_{\alpha\beta}x_\alpha x_\beta[(x - x_\alpha)/(x_\beta - x_\alpha)][(x_\beta - x)/(x_\beta - x_\alpha)]/2.$$

7(a)] rather than the entropy change [curve in Fig. 7(b)]. It is interesting to note that the present analyses (Figs. 7 and 8), which are based on experimentally obtained results, are very similar to the behavior theoretically outlined by Flanagan and Oates.[13]

It can be concluded that U plays a key role in the description of the long sloping plateau region for this stoichiometric compound. It is therefore useful to plot the phase contributions to the total change of the Gibbs free energy in various crystallographic regions (Fig. 9). As expected, the energy of the α phase is the only significant contribution in the α solid-solution region, becoming of minor importance in the two-phase coexisting region to become zero in the β solid-solution region [curve in Fig. 9(a)]. The curve in Fig. 9 (b) combines the contribution of the β-phase energy and crystal lattice. It is zero in the α solid-solution region but significant in the two-phase region, and it is the only term present in the β solid-solution region. In contrast, the Gibbs free energy of the interphase interaction [curve in Fig. 9(c)] is of major importance in the two-phase coexistence region and is zero outside this region. From this analysis it can be concluded that the newly introduced energy terms in the Hamiltonian [Eq. (15)] are essential for the proposed model to properly describe the experimental results. Additional simulations, not presented in the present paper, indeed confirmed that removing $U_{\alpha\beta}$ or L in Eq. (15) did not lead to an accurate description of the isotherms.

Consider the family of alloys $LaNi_yCu_{1.0}$, characterized by composition $y=4.0$, 4.2, 4.4, and 5.0. The stoichiometric

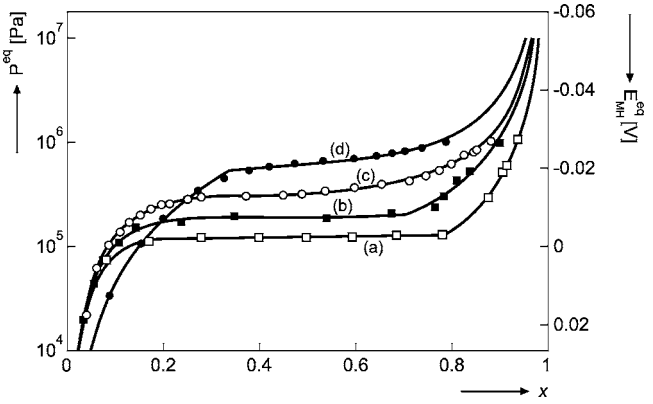

FIG. 10. Measured (symbols) and calculated (lines) pressure-composition isotherms (P_{H_2}) and equilibrium voltage (E_{MH}^{eq}) curves for various non-stoichiometric compounds as a function of composition: (a) $LaNi_{4.0}Cu_{1.0}$, (b) $LaNi_{4.2}Cu_{1.0}$, (c) $LaNi_{4.4}Cu_{1.0}$, and (d) $LaNi_{5.0}Cu_{1.0}$. All measurements have been performed via the gas phase 20 °C.[19]

composition of $LaNi_{4.0}Cu_{1.0}$ demonstrates a long and almost flat plateau region. But with an increasing degree of nonstoichiometry the miscibility gap decreases and even disappears above the as-denoted critical composition, close to $LaNi_{4.4}Cu_{1.0}$. Here, immediate phase transition is induced, as experimentally confirmed and described[19] (see, e.g., Fig. 6 herein). Above this composition only two solid-solution regions can be discerned and a two-phase coexistence region does not exist, i.e., $x_\alpha = x_\beta$.[20] Hence, a new parameter x_{tr} can be introduced, which indicates this special phase transition point. For example, Eq. (29) can then be rewritten as

$$P_{H_2} = P_{\text{ref}} \exp\begin{cases} \dfrac{2e}{kT}(E_\alpha + U_{\alpha\alpha}x) - 2\ln\left(\dfrac{1-xd}{xd}\right), & x < x_{tr}, \\ \dfrac{2e}{kT}(E_\beta + U_{\beta\beta}x) - 2\ln\left(\dfrac{1-x}{x}\right), & x \geqslant x_{tr}. \end{cases} \tag{29'}$$

On the analogy of the continuity condition given in Eq. (34), the following relationship can, in this particular case, be given

$$E_\beta = E_\alpha + (U_{\alpha\alpha} - U_{\beta\beta})x_{tr} + \frac{RT}{F}\left\{\ln\left(\frac{1-x_{tr}}{x_{tr}}\right) - \ln\left(\frac{1-x_{tr}d}{x_{tr}d}\right)\right\}. \tag{34'}$$

The complete set of calculated pressure-composition isotherms and corresponding equilibrium voltages for the various (non-)stoichiometric compounds is shown in Fig. 10. All simulation results (lines) demonstrate good agreement with the experimental data (symbols). It can be concluded that at a higher degree of nonstoichiometry, when the number of introduced dumbbell pairs increases (see Fig. 2), both the plateau pressure and the slope of the plateau increases. The calculated parameter values of the lattice gas model for all (non-)stoichiometric hydride-forming materials are represented in Table I. The values of the interaction energies are comparable to those reported in the classical paper of

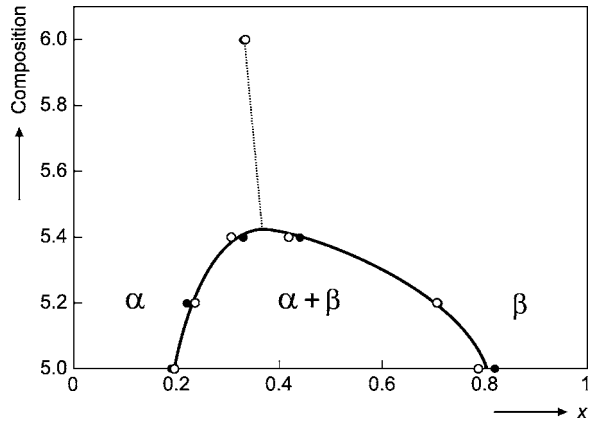

FIG. 11. Measured (open symbols) and calculated (filled symbols) phase diagram of the nonstoichiometric compounds upon hydrogen absorption (see corresponding isotherms in Fig. 10).

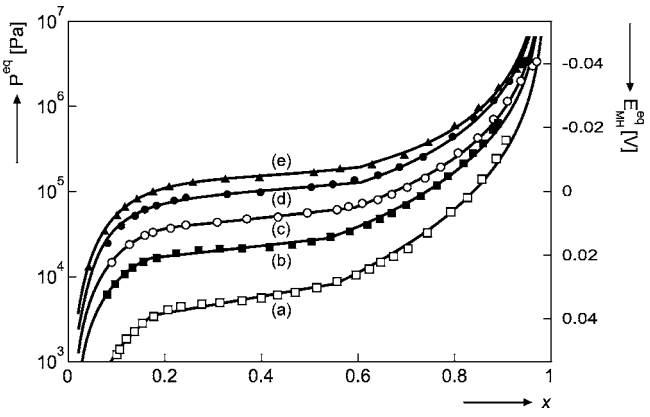

FIG. 12. Pressure-composition isotherms (P_{H_2}) and equilibrium voltage (E^{eq}_{MH}) curves for a commercial, MischMetal-based, hydride-forming electrode material at (a) 0, (b) 24, (c) 45, (d) 60, and (e) 70 °C.[30,31]

McKinnon and Haering.[3] Intraphase interaction energies were reported to range from −5 to −1 kT, corresponding to −0.129 to −0.026 eV. These values agree very well with those found in the present work (see $U_{\alpha\alpha}$ and $U_{\beta\beta}$ values in Table I). The interphase interaction energies $U_{\alpha\beta}$ are slightly higher but are still within a reasonable physical range. Some systematic changes in the obtained constants can also be observed. E_β and $U_{\alpha\alpha}$ steadily increase while, on the other hand, L, E_α and $U_{\beta\beta}$ decrease with increasing degree of nonstoichiometry. A more detailed analysis of this particular behavior is outside the scope of the present work and will be discussed in more detail in a forthcoming paper.

Figure 11 presents the estimated (filled symbols) and experimental (open symbols) phase diagrams for $LaNi_yCu_{1.0}$ hydride-forming materials. These results indeed demonstrate that the miscibility gap is clearly influenced by the nonstoichiometric composition of the hydrogen storage alloy. The simulation results are in a good agreement with the experimental data obtained from the *in situ* XRD measurements.[19,20]

Commercial MischMetal-based, AB_5-type hydride-forming material has been simulated at different temperatures.[30,31] The complete set of simulated pressure-composition isotherms at different temperatures is shown in Fig. 12. Again, the lattice-gas model demonstrates good agreement between the experimental (symbols) and theoretical (lines) results. As expected, the plateau pressure increases with increasing temperatures. The estimated parameter values of Eq. (29) are listed in Table II. Interestingly, a systematic increase of both host site energies (E_α and E_β) with temperature is clearly observed. It therefore becomes more difficult to insert hydrogen atoms at higher temperatures, which is generally accepted to occur.

Finally, the well-known principle of the minimal energy[2,3] is presented, as an example, for the MischMetal alloy at 0 °C in Fig. 13. The energies of the α [curve in Fig. 13(a)] and β phase [curve in Fig. 13(b)] are calculated based on the estimated constants and considering that phase transition at x_α and x_β did not occur. It is clearly visible, that the total Gibbs free energy of the system, as represented by the integrated form of Eq. (28), [curve in Fig. 13(c)] is lower than the partial energies of the α and β phases [curves in Figs. 13(a) and 13(b)] in the two-phase coexistence region. This indeed indicates that it is energetically more favorable for the hydrogen storage system to be in the mixed-phase state rather than in the solid-solution states. This is in line with generally accepted thermodynamic considerations.

The principles outlined in the present paper are certainly not restricted to hydrogen storage in the AB_5-type host material discussed in the present paper but can also be applied to other crystallographic host materials, such as AB_2, AB, and A_2B hydride-forming compounds.[1,32] Evidently, the model can easily be expanded when more than one phase transition is involved. In addition, other electrochemical stor-

TABLE II. Simulation results for commercial, MischMetal-based, hydride-forming electrode material at various temperatures

Temperature (°C)	x_α	x_β	E_α (eV)	E_β (eV)	$U_{\alpha\alpha}$ (eV)	$U_{\beta\beta}$ (eV)	$U_{\alpha\beta}$ (eV)	L (eV)
0	0.184	0.581	0.005	−0.033	−0.046	−0.007	−0.071	0.011
24	0.211	0.556	0.037	−0.009	−0.115	−0.025	−0.123	0.012
45	0.208	0.596	0.049	0.010	−0.123	−0.045	−0.194	0.010
60	0.235	0.603	0.060	0.022	−0.125	−0.051	−0.196	0.010
70	0.229	0.603	0.068	0.036	−0.128	−0.064	−0.235	0.009

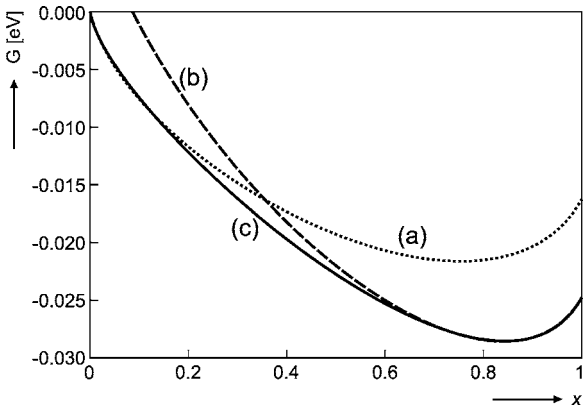

FIG. 13. Total Gibbs free energy (c) and partial energies of the (a) α phase and (b) β phase calculated for a commercial, MischMetal-based, hydride-forming material at 0 °C.[30,31]

age systems, including Li-intercalation materials, nowadays widely applied in rechargeable Li-ion batteries,[33,34] can also be described by the presented theory. These and other studies will be addressed in the near future.

IV. CONCLUSIONS

Three different stages have to be distinguished in the hydrogen absorption process: an α solid-solution region, an α-to-β two-phase coexistence region followed by a β solid solution. The presented lattice gas model is based on the Bragg-Williams approximation and the mean-field theory. A binary alloy approach has been adopted, including simple assumptions of the hydrogen concentration dependencies. A complete set of equations, describing pressure-composition isotherms and corresponding equilibrium potential curves for AB_5-type hydrogen storage materials has been obtained. The model defines the pressure and potential as explicit functions of the normalized hydrogen concentration x with eight parameters, i.e., the phase-transition points (x_α and x_β), the energies of individual hydrogen atoms (E_α and E_β), the interaction energies within the α and β phases ($U_{\alpha\alpha}$ and $U_{\beta\beta}$), the interaction energy between hydrogen atoms in the different phases ($U_{\alpha\beta}$), and the host energy (L). The isotherms consist of three parts; the first ($x<x_\alpha$) and last ($x>x_\beta$) parts characterize the solid-solution regions of the pure α and β phases, respectively, and has a Nernst-type shape, demonstrating a logarithmic behavior. The mathematical equation for the two-phase coexistence (plateau) region is a linear function of the hydrogen concentration.

Simulations of experimental absorption isotherms have been presented for both model hydride-forming $LaNi_yCu_{1.0}$-type materials and commercial MischMetal-based hydrogen storage electrode materials. The experimental and theoretical results of both the equilibrium hydrogen pressure and the equilibrium electrode potential show good agreement. The miscibility gap of the absorption isotherm is influenced by the composition of the hydride-forming material. Above a given critical composition $y \approx 4.4$ the miscibility gap is predicted to disappear. It has been analyzed that the contribution of the interaction energy between absorbed hydrogen atoms in the various phases to the Gibbs free energy is essential. The calculated pressure-composition isotherms at various temperatures also show good agreement with the experiments.

ACKNOWLEDGMENTS

The authors would like to thank Dr. E.A. Verbitskiy, Professor L.F. Feiner (Philips Research, The Netherlands) and Professor T.B. Flanagan (University of Vermont) for stimulating and helpful discussions.

*To whom correspondence should be addressed. Email address: Peter.Notten@Philips.com

[1] Y. Fukai, *The Metal-Hydrogen System* (Springer-Verlag, Berlin, 1993).
[2] T. B. Flanagan, *Thermodynamics of Metal-Gas Reactions*, Interstitial Intermetallic Alloys (Kluwer, Dordrecht, 1995), p. 43.
[3] W. R. McKinnon and R. R. Haering, *Physical Mechanism of Intercalation* (National Research Council, Canada, 1983), p. 235.
[4] P. H. L. Notten, *Interstitial Intermetallic Alloys*, edited by F. Grandjean, G. L. Long, and K. H. J. Buschow, ASI Series Vol. E281 (NATO, 1995), Chap. 7.
[5] P. H. L. Notten and M. Latroche, *Hydrogen the Energy Carrier of the Future* (Wiley, London, in press), Chap. 5.4.
[6] L. Schlapbach and A. Zuttel, Nature (London) **414**, 353 (2002).
[7] K. H. J. Buschov, P. C. P. Bouten, and A. R. Miedema, Rep. Prog. Phys. **45**, 937 (1982).
[8] R. Griessen and T. Riesterer, *Heat Formation Models*, Topics in Applied Physics Vol. 63 (Springer-Verlag, Berlin, 1988), p. 219.
[9] L. Schlapbach, *Surface Properties and Activation*, edited by L. Schlapbach, Topics in Applied Physics (Springer-Verlag, Berlin, 1992), p. 15.
[10] H. Frieske and E. Wicke, Ber. Bunsenges. Phys. Chem. **77**, 48 (1973).
[11] Y. Sakamoto, E. Kakihisa, and Y. Kinari, Z. Phys. Chem. **179**, 69 (1993).
[12] A. Ledovskikh, E. Verbitskiy, A. Ayeb, and P. H. L. Notten, J. Alloys Compd. **356-357**, 742 (2003).
[13] T. B. Flanagan and W. A. Oates. Top. Appl. Phys. **63**, 49 (1988).
[14] J. R. Lacher, Proc. Cambridge Philos. Soc. **33**, 518 (1937).
[15] S. Naito, M. Yamamoto, M. Doi, and M. Kimura, J. Chem. Soc., Faraday Trans. **22**, 4143 (1995).
[16] M. V. Lototsky, V. A. Yartys, V. S. Marinin, and N. M. Lototsky, J. Alloys Compd. **356-357**, 27 (2003).
[17] W. R. McKinnon, Chem. Sol. State Mat. **5**, 163 (1995).
[18] P. H. L. Notten, R. E. F. Einerhand, and J. L. C. Daams, J. Alloys Compd. **210**, 221 (1994)
[19] P. H. L. Notten, J. L. C. Daams, and R. E. F. Einerhand, J. Alloys Compd. **210**, 233 (1994).
[20] P. H. L. Notten, R. E. F. Einerhand, and J. L. C. Daams, J. Alloys Compd. **231**, 604 (1995).

[21] W. Coene, P. H. L. Notten, F. Hakkens, R. E. F. Einerhand, and J. L. C. Daams, Philos. Mag. A **65**, 1485 (1992).
[22] M. Latroche, J. M. Joubert, P. H. L. Notten, and A. Percheron-Guegan, J. Solid State Chem. **146**, 313 (1999).
[23] R. A. Alberty, Pure Appl. Chem. **73**, 1349 (2001).
[24] J. R. Magnus and H. Neudecker, *Matrix Differential Calculus with Applications in Statistics and Econometrics* (revised edition) (Wiley, New York, 1999).
[25] S. E. Millman and G. Kirczenow, Phys. Rev. B **28**, 3482 (1983).
[26] S. A. Safran, Phys. Rev. Lett. **44**, 937 (1980).
[27] T. L. Hill, *An Introduction to Statistical Thermodynamics* (Addison-Wesley, Reading, MA, 1960).
[28] A. Ledovskikh, E. Verbitskiy, and P. H. L. Notten, 203rd ECS Meeting, Paris, April 2003.
[29] P. H. L. Notten, A. V. Ledovskikh, E. Verbitskiy, D. Danilov, and W. Rey, MRS Fall Meeting, Boston, November 2004.
[30] H. Senoh, K. Morimoto, H. Inoue. C. Iwakura, and P. H. L. Notten, J. Electrochem. Soc. **147**, 2451 (2000).
[31] Y. Dansui and P. H. L. Notten (private communication).
[32] E. Higuchi, K. Hidaka, Z. P. Li, S. Suda, S. Nohara, H. Inoue, and C. Iwakura, J. Alloys Compd. **335**, 277 (2002).
[33] D. Danilov and P. H. L. Notten, 12th International Meeting on Lithium Batteries, Nara, Japan, June 2004.
[34] D. Danilov and P. H. L. Notten (unpublished).